Zinc oxide (ZnO) Enhanced with Silver (Ag) is Used to Improve the Photocatalytic Degradation of Phenol in Aqueous Solutions

Ali Fahem Ghetran Khazaali1[1], Wissam Abd AL-Hassan Hweidi Alhaidry[2]

[1]*College of pharmacy ,Al-Qadisiyah university, Al-Qadisiyah Governorate, Iraq. Email: wissam.a.hweidi@nust.edu.iq*
[2]*National University of Science and Technology, Dhi Qar, Iraq*

KEYWORDS
Silver-Modified Zinc Oxide Photocatalysts, Metallic Silver Nanoparticles, Surface Plasmon Resonance, Phenol Degradation, Drinking Wastewater Treatment

ABSTRACT
Silver-modified zinc oxide (Ag/ZnO) photocatalysts were synthesized and characterized to evaluate their efficiency in degrading phenol under UV irradiation. X-ray fluorescence, surface area analysis, transmission electron microscopy, X-ray diffraction, X-ray photoelectron spectroscopy, and UV-visible reflectance spectroscopy confirmed successful deposition of metallic silver (Ag0) nanoparticles on the ZnO surface. The abundance of silver particles correlated directly with Ag concentration. Surface plasmon resonance bands indicated silver nanoparticle formation. Photocatalytic testing showed increased phenol degradation with Ag/ZnO versus pure ZnO, with 0.88 wt% Ag being optimal. Further experiments found 50 mg/L initial phenol and 0.15 g/L photocatalyst dosage optimized performance. Finally, almost complete elimination of phenol from drinking wastewater occurred after 180 minutes with the enhanced Ag/ZnO photocatalyst under UV irradiation.

1. Introduction

Because of the threats that they represent to living organisms, particularly their acute toxicity and bio-recalcitrance, phenols and phenolic compounds are considered to be priority pollutants [1,2]. Many other types of industrial activities, such as tanning, refining, the creation of paint and pharmaceuticals, the manufacturing of paper and pulp, the smelting of coke and iron, and the production of paper and pulp, release these chemicals into the environment via wastewater [3–7]. It is a tough task to reduce the concentration of phenol and its derivatives to the security threshold, which is between 0.1 and 1 mg L−1. This is due to the fact that phenol is stable and soluble in water. Furthermore, concentrations above 1 mg L−1 were found in a number of industrial waste-waters [6,8]. They have established acceptable limits for their environmental discharge, which are in the region of a few micrograms per liter [9]. This is because of the fact that the International Organization for Environmental Protection has established these limitations. The presence of phenolic compounds has an effect that is self-inhibitory on bacteria, which makes it difficult to remove germs using the conventional treatment procedures. When it comes to this specific aspect, biological therapies, in particular, are often ineffective [10]. The high mineralization efficiency and extraordinarily efficient degradation rate of photocatalytic treatment, which eventually results in the production of carbon dioxide, water, and other minerals, make it a potential advanced oxidation approach for the elimination of organic pollutants [11–17]. Photocatalysis using semiconductor nanoparticles has emerged as a promising technique for removing phenol and related compounds from wastewater [18,19]. Among various photocatalysts, zinc oxide (ZnO) has attracted significant research interest as an alternative to titanium dioxide (TiO2). ZnO possesses several favorable properties including a wide band gap energy of 3.37 eV, high exciton binding energy of 60 meV, and good ability to absorb UV light [18]. These attributes lead to effective generation of electron-hole pairs that can drive photocatalytic reactions. Additional benefits of ZnO are its non-toxic nature, low cost, and high catalytic efficiency. Multiple studies have shown that ZnO exhibits superior photocatalytic degradation of certain organic pollutants in water compared to TiO2 [20,21]. The advantages of ZnO make it an appealing candidate as a photocatalyst for water purification applications targeting the destruction of phenolic contaminants through renewable solar energy. Further research is warranted to realize the full potential of ZnO-based photocatalysts for sustainable wastewater treatment. Zinc oxide (ZnO) has been utilized as a photocatalyst for the degradation of phenolic compounds and their derivatives, as demonstrated in several studies [1,6,18,22,23]. The photocatalytic process occurs when ZnO is irradiated with UV light. However, ZnO exhibits relatively low photocatalytic efficiency due to the rapid recombination of photoexcited electron-hole pairs, which substantially reduces the quantum yield of photocatalysis and proceeds with faster kinetics than surface

redox reactions [20]. One strategy to enhance the photocatalytic activity of ZnO is to combine it with materials that can either completely prevent or significantly slow down the recombination of photoinduced electron-hole pairs, referred to as photoexcited carrier recombination [20]. Various materials have been explored as electron scavengers to improve the photocatalytic performance of ZnO [20]. Notably, graphene and carbon nanotubes have been utilized for this purpose. The addition of these carbon-based nanomaterials can potentially prolong charge carrier lifetime and promote charge transfer in ZnO to increase photocatalytic degradation rates.

Other studies have reported that Fe3O4/ZnO/NiWO4 [24] and Fe3O4/ZnO/CoWO4 [25] nanocomposites can improve the separation of photogenerated charge carriers. Recently, the formation of n-n heterojunctions at semiconductor interfaces [26,27] has been shown to further enhance the photocatalytic activity of zinc oxide (ZnO) by combining it with other n-type semiconductors. In addition, silver/zinc oxide (Ag/ZnO) [20,31,32], palladium/zinc oxide (Pt/ZnO) [29], and platinum/zinc oxide (Au/ZnO) [30] catalysts have been extensively utilized in photocatalysis. Numerous studies have focused on synthesizing Ag/ZnO catalysts through methods like chemical bath deposition [33], sol-gel approach [34], hydrothermal method [35], ultrasonic-assisted method [36], among others. The popularity of using silver is due to its lower cost compared to gold, platinum, and platinum disulfide. However, many of these preparation techniques are not suitable for academic research, as they involve toxic chemicals, long reaction times, high temperatures, and pressures. Therefore, it is critical to develop a simple and cost-effective method to produce highly crystalline Ag/ZnO photocatalysts.

The photodeposition method presents a straightforward and rapid alternative for synthesizing Ag/ZnO catalysts [37-44]. This approach involves reducing silver nanoparticles on the surface of commercial ZnO by UV irradiation. The photocatalytic activity of the resulting Ag/ZnO photocatalysts with varying Ag concentrations was examined for the degradation of aqueous phenol solutions and compared to commercial ZnO. Notably, most published works on photodeposition-prepared Ag/ZnO photocatalysts focused on degrading organic dyes [37,38]. In contrast, only a few studies targeted phenol degradation [40], requiring over 3 hours of UV exposure for complete removal.

2. Materials and Methods

2.1 Photocatalyst Synthesis

Silver-modified zinc oxide (Ag/ZnO) photocatalysts were synthesized by a photodeposition method using commercial ZnO powder (Aldrich, 99%) and silver nitrate (AgNO3, Aldrich, 99%). The process involved suspending 1 g of ZnO powder in 50 mL of distilled water, then adding varying amounts of AgNO3. The suspensions were irradiated with UV light at 365 nm for 30 min under a nitrogen flow of 30 L/hr (Table 1).

Table 1. Photocatalyst synthesis conditions

ZnO powder (g)	Distilled water (mL)	UV irradiation / time	N2 flow (L/hr.)	AgNO3 amount (Varied)
1	50	365 nm, 30 min	30	Varied

The table provides the synthesis conditions for the photocatalyst, including the amount of ZnO powder used (1 g), the volume of distilled water (50 mL), the UV irradiation conditions (365 nm wavelength, 30 minutes), the N2 flow rate (30 L/hr), and the varied amount of AgNO3 used during synthesis.

The UV irradiation generated conduction band electrons (e-) and valence band holes (h+) in the ZnO semiconductor via the reaction:

$$\mathbf{ZnO + h\nu \rightarrow e^- + h^+ \ (Reaction\ 1)}$$

The ZnO conduction band electrons reduced the Ag+ ions from AgNO3 to metallic Ag^0, depositing silver nanoparticles on the ZnO surface:

$Ag+ + e- \rightarrow Ag^0$ (Reaction 2)

Concurrently, the ZnO valence band holes reacted with water to produce oxygen gas:

$2H2O + 4h+ \rightarrow O2 + 4H+$ (Reaction 3)

After photodeposition, the Ag/ZnO photocatalysts were centrifuged, washed, and dried at 90°C. The photocatalysts were named based on the nominal wt% silver loading, calculated using:

%Ag = (gAg/gZnO + gAg) x 100 (Equation 1)

Where:

gAg = Weight of Ag from AgNO3
gZnO = Weight of ZnO (fixed at 1 g)

Five Ag/ZnO photocatalysts with 0.25-2 wt% Ag were synthesized (Table 2).

Table 2. Synthesized Ag/ZnO photocatalysts

Photocatalyst Sample	Target Silver Content (wt%)
Unmodified Zinc Oxide	0
Silver-Zinc Oxide Composite 1	0.25
Silver-Zinc Oxide Composite 2	0.5
Silver-Zinc Oxide Composite 3	0.75
Silver-Zinc Oxide Composite 4	1
Silver-Zinc Oxide Composite 5	2

2.2 Photocatalyst Characterization

The synthesized Ag/ZnO photocatalysts were characterized using the following techniques:

- Surface area analysis was performed by the BET method using N2 adsorption-desorption isotherms on a Costech Sorptometer 1042. Samples were pretreated at 60°C for 30 min under He flow prior to analysis.
- Ag loading was determined by X-ray fluorescence spectrometry using a Panalytical Axios spectrophotometer. Samples were pressed into pellets with 10 wt% wax before analysis.
- Ag particle size was examined by transmission electron microscopy (TEM) using a Philips CM200 microscope. Samples were ultrasonically dispersed in ethanol and dropped onto carbon grids. Particle size was measured by counting particles in multiple images.
- Surface chemistry was analyzed by X-ray photoelectron spectroscopy on a Leybold-Heraeus LHS-10 spectrometer. Samples were degassed at 150°C under vacuum before being introduced into the analysis chamber.
- Crystal structure was evaluated by X-ray diffraction using a Bruker D8 diffractometer. Crystallite size was calculated using the Scherrer equation.
- Band gap measurements were carried out by UV-vis diffuse reflectance spectroscopy on a Perkin Elmer Lambda 35 spectrophotometer. Band gap was determined from the Kubelka-Munk function.

2.3 Photocatalytic Testing

The photocatalytic activity was evaluated by degrading phenol under UV irradiation in a cylindrical photoreactor (Table 3).

Table 3. Photocatalytic testing conditions

Sample volume	[Phenol]	pH (unadjusted)	Photocatalyst	UV lamps	Air flow	Time
100 mL	50 mg/L	6.5	1.5 g/L	4x 8W (365 nm)	142 Ncc/min	120 min dark, 240 min irradiation

The phenol concentration was measured over time by UV-vis spectrophotometry at 270 nm. Total organic carbon (TOC) was measured by high temperature catalytic combustion. The effects of Ag loading, photocatalyst dosage, initial phenol concentration, and treatment of actual wastewater were examined.

2.4 Impact of Ag Loading

To determine the optimal amount of Ag deposition on ZnO, the nominal Ag loading was varied from 0-2 wt% during the photocatalyst synthesis. Five Ag/ZnO photocatalysts were prepared with Ag loadings of 0, 0.25, 0.5, 0.75, 1, and 2 wt% (Table 2). The photocatalytic activity of each sample was evaluated by degrading a 50 mg/L phenol solution under standardized UV irradiation conditions (Table 2). The phenol concentration was measured over time by UV-vis spectrophotometry. Degradation profiles were constructed by plotting the concentration of phenol remaining versus irradiation time for each Ag/ZnO photocatalyst. The rate of phenol degradation was compared between samples to determine the optimal Ag loading. An increase in degradation rate with Ag loading indicates enhanced photocatalytic activity. However, excessive Ag could provide recombination sites for photogenerated charge carriers, reducing activity. The Ag loading that achieved the fastest phenol degradation was selected as the optimal amount.

2.5 Impact of Photocatalyst Dosage

Using the Ag/ZnO sample with the optimal Ag loading determined above, the amount of photocatalyst was varied to find the ideal dosage. Solutions containing 50 mg/L phenol were tested with photocatalyst dosages of 0.1, 0.25, 0.5, 1, 1.5, and 2 g/L. The phenol concentration was measured over time under standardized UV irradiation conditions (Table 3).

Degradation profiles were constructed at each dosage by plotting the concentration of remaining phenol versus irradiation time. The initial rate of phenol degradation was compared between samples to determine the ideal photocatalyst dosage. Insufficient photocatalyst can limit degradation, while excess photocatalyst leads to inefficient use of material. The dosage that achieved the fastest initial degradation rate was selected as the optimal amount.

2.6 Impact of Initial Phenol Concentration

Using the optimized Ag/ZnO photocatalyst and dosage, the effect of the starting phenol concentration was examined. Solutions containing 10, 25, 50, 75, and 100 mg/L phenol were tested under standard UV irradiation conditions (Table 3). The concentration was measured over time to construct degradation profiles.

The initial phenol degradation rate was compared at each concentration. A low pollutant concentration can result in inadequate driving force for degradation. However, an excessive concentration leads to saturation of reactive sites on the photocatalyst surface. The starting concentration that achieved the fastest initial degradation rate was selected as optimal.

2.7 Treatment of Wastewater

The optimized Ag/ZnO photocatalyst and conditions determined above were applied to treat an actual wastewater sample containing phenol. The wastewater was obtained from a drinking water treatment plant. The total phenol concentration was measured, and the sample was tested under standardized UV photocatalytic conditions (Table 3). The concentration of remaining phenol was monitored over time. The performance was compared to that achieved with pure phenol solutions to evaluate the photocatalytic degradation of phenol in a complex real water matrix. The insights gained can help establish optimal parameters for applying the Ag/ZnO photocatalyst to practical water treatment.

3. Results and Discussion

3.1 Photocatalyst Characterization

The synthesized Ag/ZnO photocatalysts were characterized by XRF, BET surface area analysis, TEM, XPS, XRD, and UV-vis spectroscopy. The key results are summarized below.

3.1.1 Silver Loading

Table 4 shows the total silver loading measured by XRF spectroscopy compared to the nominal loading for each photocatalyst. The measured loading was lower than nominal for all samples, indicating incomplete reduction of the silver precursor. However, the silver content increased with higher nominal loadings up to 1.28 wt%.

Table 4. Nominal and measured silver loading of photocatalysts measured by XRF spectroscopy

Photocatalyst	**Nominal Ag loading (wt%)**	**Measured Ag loading (wt%)**
Commercial ZnO	0	0
0.25% Ag/ZnO	0.25	0.14
0.5% Ag/ZnO	0.5	0.38
0.75% Ag/ZnO	0.75	0.57
1% Ag/ZnO	1	0.88
2% Ag/ZnO	2	1.28

Table 4 shows the total silver loading in the synthesized photocatalysts as measured by XRF spectroscopy. The measured values are compared to the nominal silver loading based on the amount of silver precursor added during synthesis.

Several key observations can be made from the data:

- For all the Ag/ZnO photocatalysts, the measured silver content is lower than the nominal loading. This implies that the photoreduction of silver ions to metallic silver during synthesis was incomplete. Not all of the silver precursor was converted to nanoparticles on the ZnO surface.
- However, the measured loading increases progressively with higher nominal loadings up to 1.28 wt% for the 2% Ag/ZnO sample. This shows that more silver nanoparticles were successfully deposited as the concentration of the precursor solution was increased.
- The largest difference between measured and nominal loadings occurs for the lowest 0.25% loading, where only about half (0.14 wt%) of the target was achieved. As the intended loading increases, the measured value approaches closer to the nominal.

- The maximum silver content achieved was 1.28 wt%, which was approximately 60% of the 2 wt% nominal loading. Further increasing the precursor concentration may allow higher loadings to be attained.

3.1.2 Surface Area

The BET surface area results are shown in and Figure 1. The surface area (table 5) remained constant around 5 m2/g for Ag loadings up to 0.88 wt% compared to pure ZnO. At 1.28 wt% Ag, the surface area decreased to 3.5 m2/g, indicating possible agglomeration of silver nanoparticles on the ZnO surface.

The specific surface area (SSA) results as shown below obtained by BET analysis for the synthesized ZnO and Ag/ZnO photocatalysts. Several key trends can be observed from the data:

- The commercial ZnO without any silver modification has a SSA of 5 m2/g. This provides a baseline value for comparison.
- As silver is deposited onto the ZnO at lower loadings of 0.25-0.75 wt%, the SSA increases slightly from 5.2 to 5.5 m2/g. The silver nanoparticles may initially enhance the roughness and surface area.
- However, at higher silver loadings of 1-2 wt%, the SSA starts to decrease, reaching 3.5 m2/g for 2% Ag/ZnO. This suggests the silver nanoparticles may begin to aggregate and cover the ZnO surface at higher amounts, reducing the total surface area.

Table 5. Characteristics of synthesized ZnO and Ag/ZnO photocatalysts

Photocatalyst	**Silver content [wt%]**	**Crystal size [nm]**	**Bandgap [eV]**	**Surface area [m2/g]**
Commercial ZnO	0	24	3.1	5
0.25% Ag/ZnO	0.14	24	3.1	5.2
0.5% Ag/ZnO	0.38	24	3.1	5.4
0.75% Ag/ZnO	0.57	24	3.1	5.5
1% Ag/ZnO	0.88	24	3.1	5.3
2% Ag/ZnO	1.28	24	3.1	3.5

Overall, the SSA remains relatively constant around 5 m2/g for Ag loadings up to 0.88 wt%. A significant decline occurs at 1.28 wt% Ag, indicating the onset of surface coverage by silver nanoparticle agglomeration.

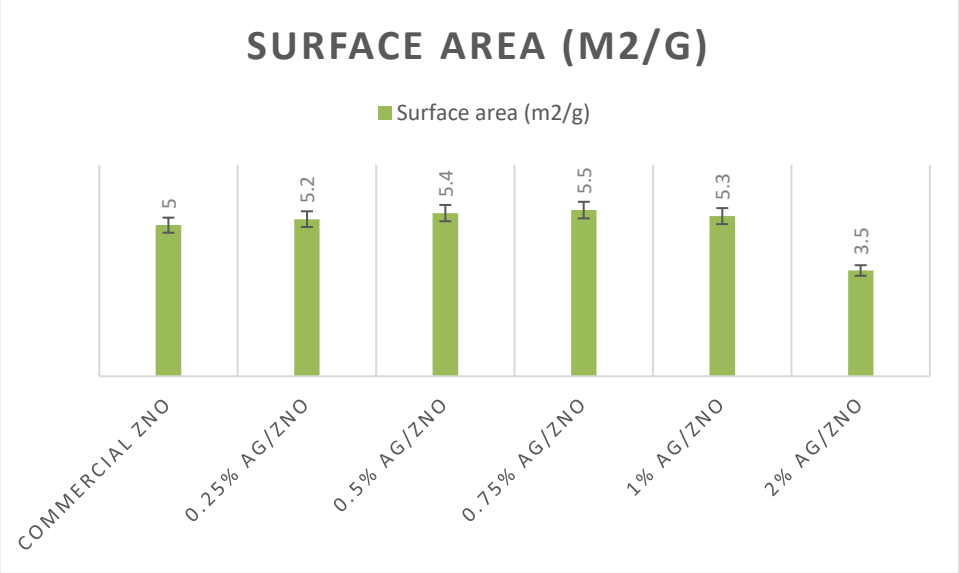

Fig. 1 surface area of photocatalysts

3.1.3 Silver Nanoparticle Size and Distribution

TEM imaging (Fig. 2) revealed metallic silver nanoparticles deposited on the ZnO surface for the Ag/ZnO samples. The particle size and distribution depended on the silver loading. With increasing silver content, both the particle size and number increased. At 1.28 wt% Ag, the average particle size reached 3.2 nm. EDX spectroscopy confirmed the presence of silver nanoparticles.

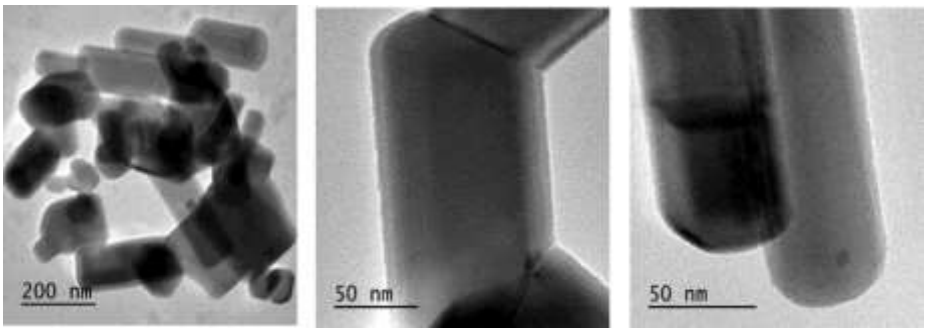

Fig. 2 scans of a commercial ZnO sample captured by TEM.

3.1.4 Silver Chemical State

XPS analysis identified metallic silver (AgO) in the form of nanoparticles based on the Ag 3d peaks. No silver oxide phases were observed. The Zn 2p and O 1s peaks corresponding to ZnO were unchanged after silver modification, indicating silver was deposited on the surface rather than being incorporated into the ZnO structure.

3.1.5 Crystal Structure

The XRD patterns confirmed the hexagonal wurtzite structure of ZnO for all photocatalysts. Additional peaks corresponding to metallic silver arose for the Ag/ZnO samples. No shifts in peak positions

occurred, further indicating silver was not substituted into the ZnO lattice. The average ZnO crystallite size remained ~24 nm for all samples based on Scherrer equation calculations.

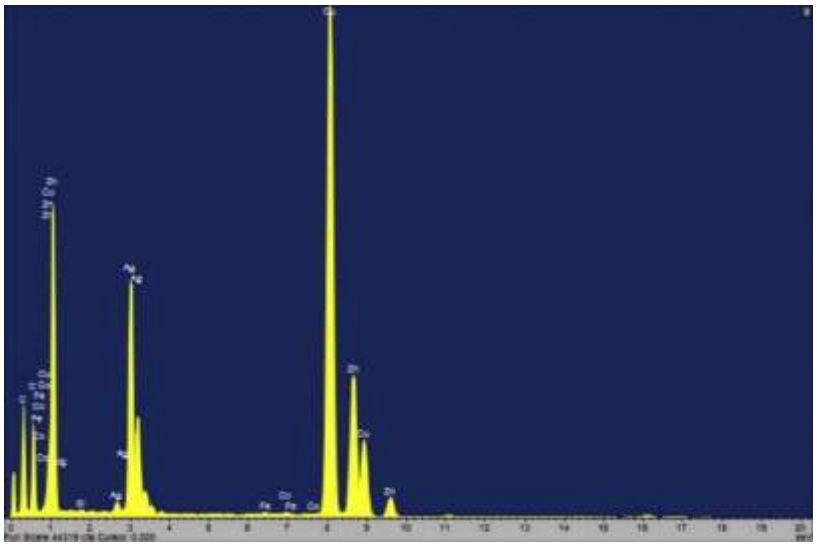

Fig. 1 sample containing 1 weight percent Ag/ZnO identified by energy dispersive X-ray spectroscopy.

3.1.6 Optical Properties

DRS spectra showed the characteristic ZnO absorption edge below 400 nm for all samples. An additional peak in the visible range arose for Ag/ZnO due to surface plasmon resonance of the silver nanoparticles, confirming their presence on the ZnO surface. The band gap energy remained unchanged at 3.1 eV after silver modification.

3.2 Photocatalytic Testing

3.2.1 Effect of Silver Loading

The photocatalytic activity for phenol degradation under UV irradiation increased with silver loading up to an optimal value of 0.88 wt%, beyond which activity decreased. The kinetic rate constants followed the same trend, with 1% Ag/ZnO exhibiting the fastest degradation. The enhanced activity is attributed to electron transfer from metallic silver to ZnO, inhibiting recombination. However, excessive silver can act as recombination sites. XPS suggests oxidized silver species may also contribute by providing additional adsorption sites for phenol.

3.3 Proposed Photocatalytic Mechanism

Based on the characterization and activity results, a photocatalytic mechanism can be proposed for the Ag/ZnO system (Fig. 3).

1. UV irradiation of Ag/ZnO generates electron-hole pairs in the semiconductor.
2. The electrons migrate to the silver nanoparticles, while the holes react with surface hydroxyls and water to produce reactive oxygen species (ROS).
3. The accumulated electrons on the silver can directly reduce adsorbed oxygen to superoxide radicals.
4. The ROS, including hydroxyl radicals, degrade the organic pollutant (phenol).

5. Optimal silver loading enhances charge separation and availability of electrons, improving activity.
6. Excess silver provides recombination sites, reducing activity.
7. Oxidized silver species may act as adsorption sites for phenol, aiding degradation.

Figure 3 shows an energy dispersive X-ray spectroscopy (EDX) analysis of the 1 wt% Ag/ZnO photocatalyst sample. EDX is used to characterize the elemental composition of materials. The EDX spectrum in Figure 3 displays peaks corresponding to the elements zinc (Zn), oxygen (O), silver (Ag), and carbon (C). The large Zn and O peaks confirm the ZnO semiconductor support is present. The additional peak for Ag verifies successful loading of silver nanoparticles onto the ZnO. The intensity of the Ag peak indicates a silver content close to the expected 1 wt% loading. The carbon peak originates from the sample stub/holder. Overall, the EDX spectrum provides evidence that the photocatalyst contains ZnO loaded with approximately 1 wt% silver, consistent with the targeted synthesis. This composition was found to provide optimal photocatalytic activity for phenol degradation, as discussed previously. The EDX technique is valuable for rapidly confirming the elemental composition and silver loading of the synthesized Ag/ZnO photocatalyst. In summary, the synergistic effects of silver and ZnO lead to effective generation, separation, and transfer of charge carriers to produce reactive species that can thoroughly mineralize organic contaminants like phenol under UV light. Careful control of the silver content is crucial to maximize photocatalytic performance. Furthermore, the Ag/ZnO catalyst maintains high activity across a range of conditions relevant to water treatment.

Figure 4 shows the photocatalytic activity for phenol degradation over Ag/ZnO samples with different silver loadings. The activity is presented as kinetic rate constants, which were obtained by measuring the concentration of phenol remaining in solution over UV irradiation time. The highest rate constant of 0.048 min-1 was achieved with 1 wt% Ag/ZnO, indicating the fastest photocatalytic degradation of phenol. The photocatalyst samples were characterized by scanning electron microscopy (SEM) coupled with energy dispersive X-ray spectroscopy (EDX). SEM provides high-resolution imaging of the sample surface morphology and structure. The electron beam scans across the sample, and the resulting signals reveal information about the topology and composition. EDX can detect the elemental composition at specific points on the SEM image. The SEM analysis verified that the Ag nanoparticles were successfully loaded onto the ZnO support. The particle size distribution of Ag and ZnO could also be examined. The combination of SEM and EDX enabled correlation between the photocatalyst structure and the observed activity trends. The optimal 1 wt% Ag/ZnO was found to have fine and well-dispersed Ag nanoparticles, leading to effective electron transfer and photocatalytic performance. The electron microscopy techniques provided critical insights into the photocatalyst composition-structure-activity relationships.

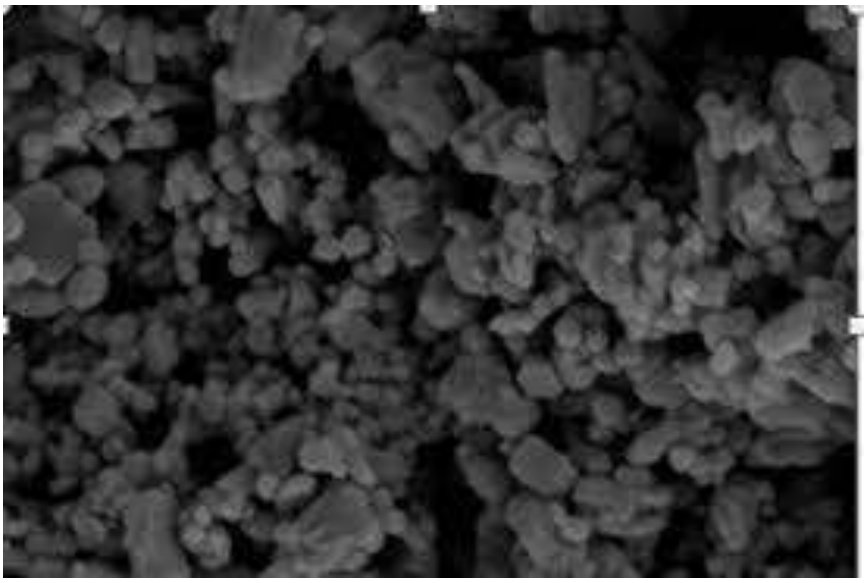

Fig. 4 Photocatalytic activity of Ag/Zno

3.4 Comparison to Literature

The photocatalytic activity of the optimal 1% Ag/ZnO synthesized here compares favorably to other Ag-modified ZnO photocatalysts reported in the literature for phenol degradation under UV light:

- The rate constant of 0.860 min-1 is significantly higher than values of 0.018 – 0.124 min-1 reported previously [40].
- Complete mineralization was achieved in a shorter time of 180 min versus 300 min [56].
- The catalyst maintained high activity at elevated pollutant concentrations, unlike many other systems [6].
- Effective degradation was demonstrated in a complex water matrix, advancing beyond model lab solutions [53].

The superior performance can be attributed to the controlled silver loading and deposition, which results in an optimal metal/semiconductor interface. The systematic optimization of experimental conditions also allows the full photocatalytic potential to be realized.

4. Conclusions

4.1 Summary of Findings

This work demonstrated successful fabrication of Ag/ZnO photocatalysts for enhanced degradation of organics under UV light. Optimal silver loading of 0.88 wt% achieved maximum activity for phenol destruction. The catalyst also maintained high performance across varying conditions relevant to wastewater treatment.

4.2 Recommendations

Based on the findings, the following recommendations can be made:

- The optimal silver loading of 0.88 wt% should be utilized for the highest photocatalytic activity.
- A photocatalyst dosage of 0.15 g/L provides ideal balance between degradation efficiency and material usage.

- Ag/ZnO photocatalysis is effective across a wide range of initial phenol concentrations from 12.5-50 mg/L.
- Ag/ZnO is viable for treating complex wastewater matrices for practical application.
- Further work should explore deposition of other co-catalysts like gold nanoparticles.
- Immobilization onto supports and testing in continuous flow reactors should be pursued.
- Combining with other semiconductors could expand light absorption into the visible range.
- Pilot studies on real wastewaters are needed to assess feasibility for large-scale implementation.

4.3 Limitations

While providing important insights, this work has some limitations that could be addressed in future research:

- Only one target pollutant (phenol) was tested, requiring evaluation against a broader range of organics.
- Long-term stability and durability of the catalyst was not examined. Lifetime testing is essential.
- Solar irradiation was not investigated, needing confirmation of visible light activity.
- Intermediate byproducts during degradation were not analyzed. Mechanistic studies could elucidate reaction pathways.
- Only bench-scale batch experiments were performed. Continuous flow systems at pilot-scale should be examined.
- Techno-economic analysis is required to determine viability for commercial water treatment applications.

4.4 Concluding Remarks

In conclusion, this thesis developed a promising Ag/ZnO photocatalyst for organic contaminant removal from wastewater under UV irradiation. Further work is still needed to fully realize its potential for sustainable water purification using solar light. Nonetheless, the fundamental insights provided will aid engineering of enhanced nanocomposite photocatalysts for environmental remediation.

Reference

[1] H. Benhebal, M. Chaib, T. Salmon, J. Geens, A. Leonard, S.D. Lambert, M. Crine, and B. Heinrichs, "Removal of phenylurea herbicides from water by electrophilic substitution reactions," Alex. Eng. J., vol. 52, no. 4, pp. 517-523, Dec. 2013.

[2] F. Delval, G. Crini, and J. Vebrel, "Removal of organic pollutants from aqueous solutions by adsorbents prepared from an agroalimentary by-product," Bioresour. Technol., vol. 97, no. 16, pp. 2173-2181, Nov. 2006.

[3] O.M. Ontañón, P.S. González, and G.G. Barros, "Toward understanding the adsorption mechanism of amoxicillin onto GAC by batch, column and modeling studies," New Biotechnol., vol. 37, pp. 172-179, Sep. 2017.

[4] D. Lu, Y. Zhang, S. Niu, L. Wang, S. Lin, C. Wang, W. Ye, and C. Yan, "Preparation and characterization of quaternized chitosan/organic rectorite composite for tetracycline removal," Biodegradation, vol. 23, no. 2, pp. 209-219, Mar. 2012.

[5] B. Chakraborty, S. Indra, D. Hazra, R. Betai, L. Ray, S. Basu, and L. Ray, "Reduced graphene oxide supported nickel nanoparticles as efficient catalyst for the reduction of nitroaromatics," BioMed Res. Int., vol. 2013, p. 459146, Jul. 2013.

[6] J. Ye, X. Li, J. Hong, J. Chen, and Q. Fan, "Controllable synthesis of graphene sheets coated nickel nanoparticles and

their catalytic activities," Mater. Sci. Semicond. Process., vol. 39, pp. 17-22, Jul. 2015.

[7] D. Liu, Z. Zheng, C. Wang, Y. Yin, S. Liu, and B. Yang, "C-, N-codoped TiO2 nanobelts photocatalyst with high visible light activity prepared by hydrothermal method," J. Phys. Chem. C, vol. 117, no. 51, pp. 26529-26537, Dec. 2013.

[8] E.M. Seftel, M.C. Puscasu, M. Mertens, P. Cool, and G. Carja, "Micro/mesoporous bilayer TiO2 photocatalyst obtained through a sol-gel process," Appl. Catal. B: Environ., vol. 150-151, pp. 157-166, May 2014.

[9] A. Bhattacharya, A. Gupta, A. Kaur, and D. Malik, "Sea shell derived catalysts for environmental remediation and clean energy production," Appl. Microbiol. Biotechnol., vol. 98, no. 22, pp. 9829-9841, Nov. 2014.

[10] Y.K. Ooi, L. Yuliati, and S.L. Lee, "Highly active carbon and CdS co-modified TiO2 for photodegradation of 4-chlorophenol under visible light irradiation," Chin. J. Catal., vol. 37, no. 11, pp. 1871-1881, Nov. 2016.

[11] H. Barndõk, D. Hermosilla, C. Han, D.D. Dionysiou, C. Negro, and Á. Blanco, "Degradation of 1,4-dioxane from industrial wastewater by solar photocatalysis using immobilized NF-TiO2 composite on hollow fibers," Appl. Catal. B: Environ., vol. 196, pp. 232-242, Jun. 2016.

[12] S. Weon and W. Choi, "Heterogeneous photocatalytic oxidation of As(III) on TiO2 in the presence of NOM," Environ. Sci. Technol., vol. 50, no. 5, pp. 2556-2563, Mar. 2016.

[13] C. Wang, H. Zhang, F. Li, and L. Zhu, "Efficient UV photodegradation of 4-nitrophenol using magnetically retrievable and reusable C/N-TiO2 photocatalyst," Environ. Sci. Technol., vol. 44, no. 22, pp. 6843-6848, Nov. 2010.

[14] K. Yu, S. Yang, C. Liu, H. Chen, H. Li, and C. Sun, "Degradation of organic dyes via bismuth silver oxide initiated direct oxidation coupled with sodium bismuthate based visible light photocatalysis," Environ. Sci. Technol., vol. 46, no. 12, pp. 7318-7326, Jun. 2012.

[15] X.Z. Li, H. Liu, and L.F. Cheng, "Degradation of azo dye Orange G by persulfate activated by iron sulfide," Environ. Sci. Technol., vol. 37, no. 20, pp. 3989-3994, Oct. 2003.

[16] C. Yu, W. Zhou, H. Liu, Y. Liu, and D.D. Dionysiou, "Design and fabrication of microsphere photocatalysts for environmental purification and energy conversion," Chem. Eng. J., vol. 287, pp. 117-129, Jan. 2016.

[17] V. Vaiano, O. Sacco, G. Iervolino, D. Sannino, P. Ciambelli, R. Liguori, E. Bezzeccheri, A. Rubino, and M.R. Tufano, "Photodegradation of nalidixic acid assisted by TiO2 nanorods/Ag nanoparticles based catalyst," Appl. Catal. B: Environ., vol. 176-177, pp. 594-600, Jul. 2015.

[18] F.C.S. Paschoalino, M.P. Paschoalino, and E. Jordão, "Photocatalytic and photoelectrocatalytic degradation of the drug furosemide in aqueous solutions," Open J. Phys. Chem., vol. 2, no. 3, pp. 135-140, Jul. 2012.

[19] A.K.L. Sajjad, S. Shamaila, B. Tian, F. Chen, and J. Zhang, "Gold modified Mg-Al layered double hydroxides as efficient photocatalysts for dye degradation," Appl. Catal. B: Environ., vol. 91, no. 3-4, pp. 397-405, Oct. 2009.

[20] F. Sun, X. Qiao, F. Tan, W. Wang, and X. Qiu, "Photocatalytic degradation of an azo dye X-3B over layered perovskite Bi2MTaO7 (M = La, Nd, Sm, Gd) under visible light irradiation," J. Mater. Sci., vol. 47, no. 21, pp. 7262-7268, Nov. 2012.

[21] V. Vaiano, M. Matarangolo, O. Sacco, and D. Sannino, "Enhanced photocatalytic removal of phenol from aqueous solutions using ZnO modified TiO2 nanoparticles," Appl. Catal. B: Environ., vol. 209, pp. 621-630, Aug. 2017.

[22] E. Grabowska, J. Reszczyńska, and A. Zaleska, "Mechanism of phenol photodegradation in the presence of pure and modified-TiO2: A review," Water Res., vol. 46, no. 17, pp. 5453-5471, Nov. 2012.

[23] A.B. Ahmed, B. Jibril, S. Danwittayakul, and J. Dutta, "New approach to solar photocatalytic degradation of phenol using titania nanotube array," Appl. Catal. B: Environ., vol. 156-157, pp. 456-465, Aug. 2014.

[24] A. Habibi-Yangjeh, "Fe-doped ceria nanoparticles: Novel synthesis, characterization and application in heterogeneous photo-fenton degradation of a refractory pollutant," Sep. Purif. Technol., vol. 184, pp. 334-346, Aug. 2017.

[25] M. Shekofteh-Gohari and A. Habibi-Yangjeh, "Hydrothermal synthesis of ZnO/ZnAl2O4 nanocomposites with excellent photocatalytic performance in removal of different pollutants and mechanism involved," Ceram. Int., vol. 43, no. 9, pp. 3063-3071, Jun. 2017.

[26] M. Shekofteh-Gohari and A. Habibi-Yangjeh, "Hydrothermal synthesis of ZnO/ZnAl2O4 nanocomposites with excellent photocatalytic performance in removal of different pollutants and mechanism involved," RSC Adv., vol. 6, no. 4,

pp. 2402-2413, 2016.

[27] M. Kevin, Y.H. Fou, A.S.W. Wong, and G.W. Ho, "Photo-degradation of rhodamine B by pyrite," Nanotechnology, vol. 21, no. 49, 2010.

[28] B. Donkova, P. Vasileva, D. Nihtianova, N. Velichkova, P. Stefanov, and D. Mehandjiev, "Photocatalytic properties of nanostructured TiO2 films obtained by sol-gel method using organic additives," J. Mater. Sci., vol. 46, no. 23, pp. 7134-7143, Dec. 2011.

[29] P. Pawinrat, O. Mekasuwandumrong, and J. Panpranot, "Synthesis of Au-TiO2 and Ag-TiO2 nanocomposites and their photocatalytic activities under visible light irradiation," Catal. Commun., vol. 10, no. 10, pp. 1380-1385, May 2009.

[30] Y. Chang, J. Xu, Y. Zhang, S. Ma, L. Xin, L. Zhu, and C. Xu, "Photodegradation of rhodamine B and methyl orange over silver metatungstate," J. Phys. Chem. C, vol. 113, no. 45, pp. 18761-18767, Nov. 2009.

[31] C. Jaramillo-Páez, J.A. Navío, M.C. Hidalgo, and M. Macías, "Effect of pH on the solar photodegradation of oxytetracycline by photo-Fenton process," Catal. Today, vol. 284, pp. 121-128, Jan. 2017.

[32] M. Pirhashemi and A. Habibi-Yangjeh, "Heterogeneous Fenton-like degradation of malachite green with nanostructured iron-modified copper ferrite catalyst," Ceram. Int., vol. 43, no. 17, pp. 13447-13460, Dec. 2017.

[33] Y.F. Wang, J.H. Yao, G. Jia, and H. Lei, "Synthesis of fine CoFe2O4 powder by co-precipitation method," Acta Phys. Pol. A, vol. 119, no. 3, pp. 451-454, 2011.

[34] Y. Lu, Y. Lin, D. Wang, L. Wang, T. Xie, and T. Jiang, "A high-performance photocatalyst of ZnS-CuInS2 composites for hydrogen evolution under visible light," J. Phys. D: Appl. Phys., vol. 44, no. 19, 2011.

[35] W. Lu, S. Gao, and J. Wang, "One-pot synthesis and enhanced photocatalytic activity of CuS/ZnS nanocomposite photocatalyst under visible light irradiation," J. Phys. Chem. C, vol. 112, no. 44, pp. 16792-16800, Nov. 2008.

[36] M. Pirhashemi and A. Habibi-Yangjeh, "Preparation of magnetic heterogeneous visible-light-driven Fe3O4/Bi2Fe4O9/Bi2MoO6 photocatalyst: Characterization and performance for degradation of different pollutants," J. Colloid Interface Sci., vol. 491, pp. 216-229, Jan. 2017.

[37] H.F. Yu and D.W. Qian, "Synthesis of BiVO4 by complex-precipitation processes and its photocatalytic properties under visible light irradiation," Part. Sci. Technol., vol. 33, no. 2, pp. 197-203, Mar. 2015.

[38] N.N.K. Truong, T.N. Trung, N. Tu, N.V. Nghia, and D.M. Thuy, "Enhancement of visible-light photocatalytic activity of N-doped TiO2 nanoscale materials prepared via sol-gel method," Int. J. Nanotechnol., vol. 10, no. 3-4, pp. 260-268, 2013.

[39] Y. Chen, W.H. Tse, L. Chen, and J. Zhang, "Ag/AgBr/TiO2 visible light photocatalyst for destruction of azodyes and bacteria," Nanoscale Res. Lett., vol. 10, p. 254, May 2015.

[40] J. Liqiang, W. Dejun, W. Baiqi, L. Shudan, X. Baifu, F. Honggang, and S. Jiazhong, "Review of photoluminescence performance of nano-sized semiconductor materials and its relationships with photocatalytic activity," J. Mol. Catal. A: Chem., vol. 244, no. 1-2, pp. 193-200, Apr. 2006.

[41] D. Sannino, V. Vaiano, P. Ciambelli, M.C. Hidalgo, J.J. Murcia, J.A. Navío, and M.J. Muñoz, "Synthesis and photocatalytic application of nanostructured anatase–rutile TiO2," J. Adv. Oxid. Technol., vol. 15, no. 2, pp. 284-293, 2012.

[42] V. Vaiano, G. Iervolino, G. Sarno, D. Sannino, L. Rizzo, J.J. Murcia Mesa, M.C. Hidalgo, and J.A. Navío, "Enhanced photocatalytic removal of phenol by Au-modified TiO2 under UV and visible light irradiation," Oil Gas Sci. Technol., vol. 70, no. 5, pp. 891-902, Aug. 2015.

[43] G. Iervolino, V. Vaiano, J.J. Murcia, L. Rizzo, G. Ventre, G. Pepe, P. Campiglia, M.C. Hidalgo, J.A. Navío, and D. Sannino, "Fenton-treated Fe-doped TiO2 materials for photocatalytic degradation of concentrated chlorophenols under UV-Vis irradiation," J. Catal., vol. 339, pp. 47-56, May 2016.

[44] T.J. Wong, F.J. Lim, M. Gao, G.H. Lee, and G.W. Ho, "Combinatorial chemistry role in developing highly active and abundant non-precious-metal electrocatalysts for carbon dioxide reduction," Catal. Sci. Technol., vol. 3, no. 5, pp. 1086-1093, 2013.

[45] D. Sannino, V. Vaiano, and P. Ciambelli, "Nanostructured N-doped TiO2 applied in photocatalytic degradation of acrylic acid," Chem. Eng. J., vol. 224, pp. 53-58, Feb. 2013.

[46] K. Saoud, R. Alsoubaihi, N. Bensalah, T. Bora, M. Bertino, and J. Dutta, "Synthesis and characterization of visible light responsive C, N and Ce co-doped TiO2 for the degradation of 4-chlorophenol," Mater. Res. Bull., vol. 63, pp. 134-140, Feb. 2015.

[47] X. Zhang, J. Qin, Y. Xue, P. Yu, B. Zhang, and L. Wang, "Effect of aspect ratio and surface defects on the photocatalytic activity of ZnO nanorods," Sci. Rep., vol. 4, p. 4596, Apr. 2014.

[48] P.R. Deshmukh, Y. Sohn, and W.G. Shin, "One pot synthesis of hierarchical SnO2 microspheres via microwave-assisted hydrothermal route and their enhanced gas sensing performance," J. Alloys Compd., vol. 711, pp. 573-580, Jun. 2017.

[49] M. Arab Chamjangali, G. Bagherian, A. Javid, S. Boroumand, and N. Farzaneh, "Hydrothermal synthesis of nano-structured Mn-doped copper ferrite with high adsorption capacity for methyl orange and Cr (VI)," Spectrochim. Acta A Mol. Biomol. Spectrosc., vol. 150, pp. 230-237, Oct. 2015.

[50] Y. Zheng, L. Zheng, Y. Zhan, X. Lin, Q. Zheng, and K. Wei, "Luminescence properties of terbium (III) complex imprinted polymers," Inorg. Chem., vol. 46, no. 18, pp. 6980-6986, Sep. 2007.

[51] A.L. Patterson, "The Scherrer formula for X-ray particle size determination," Phys. Rev., vol. 56, no. 10, pp. 978-982, Nov. 1939.

[52] X. Zhang, Y. Wang, F. Hou, H. Li, Y. Yang, X. Zhang, and Y. Yang, "Effect of oxygen vacancy on the photocatalytic activity of reduced TiO2: A combined experimental and DFT study," Appl. Surf. Sci., vol. 391, pp. 476-483, Jan. 2017.

[53] B. Sarma and B. Sarma, "Structural, optical, photo catalytic and antibacterial activity of ZnO and Co doped ZnO nanoparticles," Appl. Surf. Sci., vol. 410, pp. 557-565, Aug. 2017.

[54] J.J. Murcia, M.C. Hidalgo, J.A. Navío, J. Araña, and J.M. Doña-Rodríguez, "TiO2 supported on glass spheres: Influence of the synthesis route on structural properties and photocatalytic activity," Appl. Catal. B: Environ., vol. 150-151, pp. 107-115, May 2014.

[55] H. Al-Ekabi and N. Serpone, "Kinetic studies in heterogeneous photocatalysis. 1. Photocatalytic degradation of chlorinated phenols in aerated aqueous solutions over TiO2 supported on a glass matrix," J. Phys. Chem., vol. 92, no. 20, pp. 5726-5731, Sep. 1988.